Brodogradnja Volume 76 Number 3 (2025) 76306

journal homepage: www.brodogradnja.fsb.hr

Brodogradnja

An International Journal of Naval Architecture and Ocean Engineering for Research and Development

Multi-disciplinary optimization of underwater vehicles based on a dynamic proxy model

Shaojun Sun[1,2], *Weilin Luo*[1,2*]

[1] *Fuzhou Institute of Oceanography, Fuzhou University, Fuzhou 350108, China*
[2] *College of Mechanical Engineering and Automation, Fuzhou University, Fuzhou 350108, China*

ARTICLE INFO

Keywords:
Underwater vehicle
Dynamic proxy model
K and T indices
Collaborative optimization
Hydrodynamics

ABSTRACT

This paper presents a method for optimizing the multidisciplinary shape design of underwater vehicles using a dynamic proxy model. The method employs a collaborative optimization approach that considers various disciplines, including rapidity, maneuverability, energy consumption, and structural strength of the underwater vehicle. The K and T indices are effectively utilized to represent the maneuverability performance of underwater vehicles. The hydrodynamics of underwater vehicles are analyzed using the Computational Fluid Dynamics (CFD) numerical simulation method. To reduce the computational burden in the optimization loop, this paper proposes a dynamic proxy model that combines the trust region with the adaptive minimum confidence Lowest Credible Bound (LCB) and the Synthetic Minority Over-Sampling Technique (SMOTE) algorithm. Additionally, an adaptive balance constant is introduced into the proxy model. The collaborative optimization framework employs a combined optimization algorithm based on the genetic algorithm and Nonlinear Programming by Quadratic Lagrangian Programming (NLPQLP) algorithm. The results of applying this optimization strategy to the SUBOFF model demonstrate its effectiveness in optimizing the resistance, mass, maneuverability, structural strength, and energy consumption of the underwater vehicle.

1. Introduction

Exploring and developing the ocean has always been crucial for humans, and underwater vehicles play a vital role in this exploration process. Improving the performance of these vehicles has proven to be a challenging task. Key performance indicators include maneuverability, rapidity, energy consumption, and lightweight. However, a paradox arises when considering these indicators simultaneously. For instance, achieving good maneuverability is often feasible, but ensuring good rapidity can be challenging. The traditional single-discipline coupling method fails to adequately represent the overall performance of underwater vehicles. Multi-disciplinary design optimization (MDO) integrates multiple disciplines to provide effective solutions. MDO has been widely applied in aerospace engineering and ship engineering. Zhou et al. [1] Apply collaborative optimization to Marine engineering. Hart and Vlahopoulos [2] use PSO

* Corresponding author.
E-mail address: wlluo@fzu.edu.cn

http://dx.doi.org/10.21278/brod76306
Received 09 October 2024; Received in revised form 27 April 2025; Accepted 21 May 2025
Available online 28 May 2025
ISSN 0007-215X; eISSN 1845-5859

(particle swarm optimization) algorithm to ship design. Zhang [3] uses the MDO method to ship design. This approach is also applicable to underwater vehicles [4].

The advanced method for multidisciplinary optimization design uses CFD and the Finite Element Method (FEM). CFD saves costly experiments and provides accurate results. For example, Mikulec and Piehl [5] conducted CFD numerical simulation of the ship. Liu et al. [6] performed CFD numerical simulation on the temperature of container ships. Bal and Bural [7] analyzed the force of offshore piles through CFD numerical simulation. In MDO, proxy models are often used alongside CFD to reduce computational costs. Proxy models effectively address challenges in large engineering projects. Alvarez et al. [8] utilized the simulated annealing algorithm to conduct multidisciplinary design optimization for underwater vehicles. Gao et al. [9] employed the Multi-Island Genetic Algorithm (MIGA) for multidisciplinary design optimization of Autonomous Underwater Vehicles (AUVs). The results demonstrated that the MIGA algorithm outperformed the Particle Swarm Optimization (PSO) algorithm in terms of performance. Ignacio et al. [10] analyzed Autonomous Underwater Vehicles (AUVs) by combining CFD numerical simulation analysis with empirical methods. However, when using CFD numerical simulation technology for the shape design of underwater vehicles, a large number of high-fidelity sample points are often required. This is especially true for multidisciplinary coupling and high-dimensional optimization problems, where high-fidelity sample points demand significant computational time, which can substantially impact the optimization efficiency of underwater vehicles. To address this issue, the application of proxy models has proven to be of great importance.

Alam et al. [11] employed the Non-dominated Sorting Genetic Algorithm (NSGA-II) and the Infeasibility-Driven Evolutionary Algorithm (IDEA) to optimize the drag design of Autonomous Underwater Vehicles (AUVs). Alam et al. [12] utilized CFD and low-fidelity models to optimize the drag design of underwater vehicles. Tian et al. [13] utilized Backpropagation Neural Networks (BP) for drag discipline design of underwater vehicles. Li et al. [14] developed an approximate model based on Ellipsoidal Basis Function (EBF) neural networks to achieve lightweight design of underwater vehicles while meeting strength requirements. Previous studies primarily focused on drag reduction design for underwater vehicles, with an emphasis on optimizing the speed of Autonomous Underwater Vehicles (AUVs). Some research has also incorporated both speed and energy consumption optimization. As well as conducting standalone lightweight design for underwater vehicles. However, under complex oceanic conditions, designing speed, energy consumption, or structural strength individually is not sufficient. Poor maneuverability of underwater vehicles in challenging sea states can lead to severe maritime disasters. When an underwater vehicle is traveling at high speed and encounters obstacles, its initial turning capability and the improvement of its minimum turning radius become crucial. Additionally, AUVs are often required to perform deep-sea operations, highlighting the importance of the safety and pressure resistance of their pressure-resistant hulls. In complex oceanic conditions, optimal performance of underwater vehicles can only be achieved by simultaneously considering speed, maneuverability, energy efficiency, and structural strength. This is particularly crucial for ensuring that the vehicle maintains high speed while exhibiting superior maneuverability, safely navigating along its designated route. Additionally, it must possess robust endurance capabilities and a pressure-resistant hull that ensures safety under high water pressure.

Luo and Lyu [15] utilized static proxy models and combinatorial optimization algorithms to optimize the hydrodynamics of underwater vehicles. This method reduced computational effort and prevented the optimization process from becoming trapped in local optima. Common static proxy models for these scenarios include Radial Basis Function (RBF), Kriging, and Artificial Neural Networks (ANN). However, Conventional proxy models require an excessive number of sample points, making them insufficiently efficient for underwater vehicle engineering.

Especially for high-dimensional, complex problems involving multidisciplinary coupling, static proxy models often exhibit inefficiency and suffer from the curse of dimensionality. This is particularly evident in models such as Polynomial Response Surface (PRS), Kriging, and Response Surface Methodology (RSM).

Thus, new proxy models have been proposed. Yang et al. [16] introduced the Single-Loop Local Adaptive Kriging Model, which was validated on an underwater vehicle's pressure-resistant hull. Wang et al.

[17] applied the Gaussian algorithm for multi-disciplinary ship design optimization. Chen et al. [18] combined multiple proxy models to create an adaptive ensemble proxy model. Compared to other proxy models, it achieves higher prediction accuracy for low-dimensional functions. Validated with underwater vehicles, the model demonstrated high predictive accuracy. Enhancing optimization efficiency for underwater vehicles has been a persistent challenge. A new method for selecting sample points has proven effective. Dynamic proxy models utilize this innovative sampling method. Where points continuously update and iterate, effectively selecting highly correlated samples and achieving high model accuracy with fewer samples. Luo and Guo [19] optimized underwater vehicle resistance and energy consumption using a dynamic proxy model based on the minimum confidence region. Pan and Luo [20] optimized underwater vehicle rapidity, energy consumption, and structural strength using a dynamic proxy model updated with the SMOTE algorithm. Research indicates that integrating MDO with dynamic proxy models enhances optimization efficiency and performance of underwater vehicles. Liu et al. [21] combined the regression Kriging model with an artificial neural network agent model to design the underwater vehicle, The results showed that the global design quickly converges to a narrow range, while the local design achieves high efficiency. Although current dynamic proxy models can improve optimization efficiency, they are often compared only to static proxy models. Few studies have compared dynamic proxy models with other types of dynamic proxy models to demonstrate superior efficiency and accuracy. Additionally, existing underwater vehicle designs often fail to balance efficiency with multidisciplinary coupling. While efficiency may be improved, these designs typically focus on drag or energy consumption alone or involve limited disciplinary coupling.

To address these gaps, this study compares a static proxy model with two dynamic proxy models. The proposed proxy model demonstrates the highest design efficiency and superior fitting accuracy. Moreover, it achieves collaborative optimization across four disciplines, enhancing the robustness of underwater vehicles in complex sea conditions.

In this study, a dynamic proxy model integrating the minimum confidence lower bound with the SMOTE algorithm is employed within a collaborative optimization framework. Various disciplines, including rapidity, maneuverability, energy consumption, and structural strength, are optimized. The weights of these disciplines are effectively determined using the Analytic Hierarchy Process (AHP) method. To avoid local optima during optimization, a combined algorithm based on genetic algorithms and NLPQLP is utilized. The hydrodynamic coefficients of the underwater vehicle are calculated, and the K and T indices are obtained to evaluate its maneuverability. This article introduces the E1619 propeller and suggests using the K and T indices to accurately represent the maneuverability performance of underwater vehicles based on optimization results. For the first time, a dynamic proxy model was used to optimize the control performance of underwater vehicles, and the hydrodynamic coefficients with various rudder angles were determined. Calculating the K and T indices before and after optimization demonstrated improved control performance in underwater vehicles.

2. Underwater vehicle model

The SUBOFF model, developed by the U.S. Department of Defense, is shown in Figure 1. The mathematical model and experimental results are available. Key features include total length (L), parallel midship length (L_p), after-body length (L_{ap}), afterbody cap length (L_{cp}), parallel midship radius (R), maximum sail thickness (Z), forebody length (L_{bp}), and conning tower position (h_2).

The hydrodynamic coefficients of an underwater vehicle can be determined through numerical simulations. Numerical simulation of propellers can also be conducted by CFD. Carrica et al. [22] calculated the efficiency of propeller propulsion. Choi et al. [23] used CFD numerical simulation to calculate the resistance of ships. Ghassemi and Ghadimi [24] calculated the hydrodynamic performance of the propeller. Wu et al. [25] conducted numerical simulation of ship maneuvering performance. Wu [26] calculated the body force of the propeller using CFD. Ardeshiri and Mousavizadegan [27] proposed a method for calculating the maneuverability coefficient and applied it to underwater vehicles. The E1619 propeller, selected for these simulations [28], is geometrically represented in Figure 2.

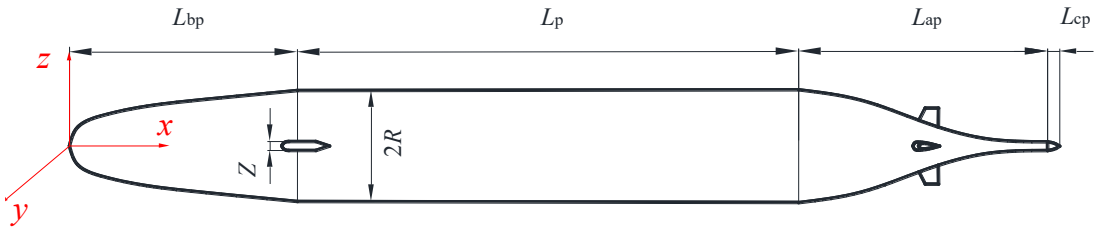

Fig. 1 SUBOFF model

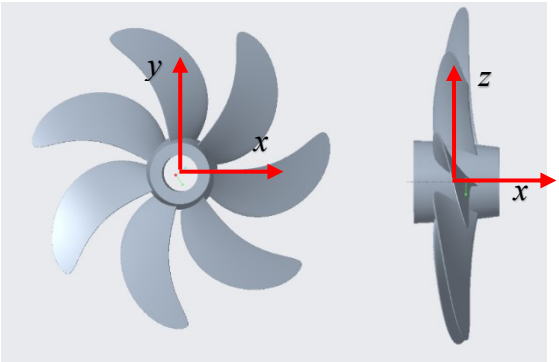

Fig. 2 E1619 propeller

The equation for the blade line of the propeller is as follows [25]:

$$y = \frac{r}{R}\cos\left(\theta_s + k\frac{2\pi}{n_b}\right) \tag{1}$$

$$z = \frac{r}{R}\sin\left(\theta_s + k\frac{2\pi}{n_b}\right) \tag{2}$$

where $n_b = 1,2,...,N$. θ_s represents the propeller skew; R denotes the maximum half-chord length, which is the distance from the propeller centerline to the leading edge of the airfoil; r is the half-chord length, which is the distance from the propeller center to the leading edge of the airfoil. k is the shape factor of the propeller. When (k = 1), a chord line is generated. After generating the chord, create the leading and trailing edges using the following equation:

$$y = \frac{r}{R}\cos\left(\theta_s + k\frac{2\pi}{n_b} \pm \theta\right) \tag{3}$$

$$z = \frac{r}{R}\sin\left(\theta_s + k\frac{2\pi}{n_b} \pm \theta\right) \tag{4}$$

$$\theta = 2\pi\frac{C}{D_p} / \sqrt{(2\pi\frac{r}{R})^2 + (2\frac{P}{D_p})^2} \tag{5}$$

where P represents the pitch, D_p is the propeller diameter; C represents the propeller blade profile, with dimensionless chord length and pitch represented by C/D_p and P/D_p, respectively; and θ represents the skew angle.

To generate a 3D geometric model, coordinate transformation is required. The steps are as follows:

$$x = R_i \cos\left(\frac{Y_1 \cos\varphi - Z_1 \sin\varphi + L\cos\varphi}{R_i}\right) \tag{6}$$

$$y = R_i \sin\left(\frac{Y_1 \cos\varphi - Z_1 \sin\varphi + L\cos\varphi}{R_i}\right) \tag{7}$$

where R_i is the radius of the cylindrical surface at different blade sections, φ is the helix angle, and Y_i and Z_i are the coordinates of any point in the local coordinate system.

For the center of the propeller, (x, y, z) represent the coordinate values of any point on the surface. Points (x_L, y_L, z_L) and (x_T, y_T, z_T) correspond to the leading edge and trailing edge points, respectively. The sectional leading edge and trailing edge angles on the propeller disk plane relative to the blade reference line are denoted as θ_L and θ_T, respectively:

$$\theta_L = \tan^{-1}(y_L / z_L) \tag{8}$$

$$\theta_T = \tan^{-1}(y_T / z_T) \tag{9}$$

3. Discipline analysis

This study optimizes rapidity, manoeuvrability, energy consumption, and structural strength. Numerical simulations analyze rapidity, manoeuvrability, and structural strength, while energy consumption is calculated from the simulation results.

3.1 Rapidity

The resistance of underwater vehicles often indicates their rapidity. Numerical simulations are used to analyze these vehicles. In fluid dynamics simulations, partitioning the flow field is necessary. A flow field domain that is too large reduces calculation efficiency. while a domain that is too small affects the accuracy of the numerical simulation. After conducting an independence analysis, this study selects a semi-circular shape for the front part of the flow field domain and a cylindrical shape for the back part, with the diameter equal to the total length of a SUBOFF. The flow field domain is shown in Figure 3.

In numerical simulation research, the first step is to establish conceptual, mathematical, and numerical simulation models. Then, the numerical simulation model is run dynamically, and the results are presented, analyzed, and explained. Both turbulent and laminar flow models are essential for dynamic simulations. This paper uses the Renormalization Group (RNG) turbulence model to validate the accuracy of CFD simulations for flow in a straight channel. Table 1 shows the correlation between the simulation and experimental values, confirming the viability of the numerical simulation.

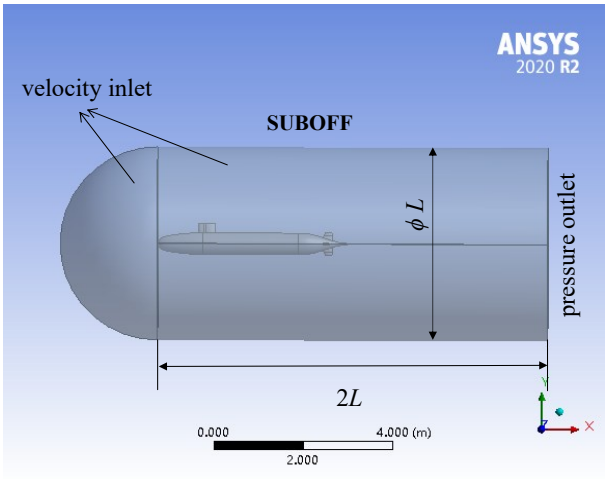

Fig. 3 Flow field region

Table 1 Underwater vehicles resistance

V (kn)	CFD (N)	Experiment (N)	Error (%)
5.93	99	102.3	3.23
10	272.8	283.8	3.88
11.85	399.3	389.2	2.60
13.92	541.1	526.6	2.75
16	704	675.6	4.20

3.2 Manoeuvrability

Marine vehicle manoeuvrability significantly impacts navigation safety and economy. Poor manoeuvrability can lead to marine disasters and accidents, posing serious safety risks. It refers to the ability to maintain or change the vehicle's motion state under control. This includes maintaining a steady speed in a straight line or adjusting the heading, speed, and position based on the helmsman's instructions. Good manoeuvrability means that the marine vehicle can sustain a constant speed and direction without manual control, even in the presence of disturbances, and can stabilize on a new heading. To change direction efficiently, optimizing manoeuvrability is essential for the vehicle to execute quick turns in response to control inputs. Lateral force and yaw moment do not adequately represent the manoeuvrability of underwater vehicles. Instead, K and T indices provide a more accurate representation:

$$K \approx -\frac{N_\delta}{N_r} \tag{10}$$

$$\begin{cases} T_1 + T_2 \approx -\dfrac{I_z - N_{\dot r}}{N_r} - \dfrac{m - Y_{\dot v}}{Y_v} \\ T_3 \approx -\dfrac{m - Y_{\dot v}}{Y_v} \\ T = T_1 + T_2 - T_3 \approx -\dfrac{I_z - N_{\dot r}}{N_r} \end{cases} \tag{11}$$

where m represents the mass of the underwater vehicle, $N_\delta, N_r, N_{\dot{r}}, Y_v, Y_{\dot{v}}$ represents the hydrodynamic derivatives, and I_z represents the inertia moment of the underwater vehicle. According to manoeuvrability theory, a larger K index indicates better turning ability, while a smaller T index indicates better initial turning ability.

As shown in equation (11), calculating K and T requires determining hydrodynamic forces, such as sway force and yaw moment, which can be obtained using CFD simulation. To generate analytical data points for the derivative of the yaw moment with respect to velocity in underwater vehicles, the velocity ranges from -5 m/s to 5 m/s in increments of 0.5 m/s. An interpolation function is constructed to calculate the derivative value at r=0, denoted as N_r.The derivative of the yaw moment with respect to acceleration is obtained using the difference method $a = \Delta v / \Delta T$. The velocity ranges from -5 m/s to 5 m/s in increments of 0.5 m/s, with a time step of 0.5 s. The derivative values of the moment with respect to the rudder angle are determined for rudder angles between -10° and 10°. Moment is generated by propeller propulsion, which is primarily simulated using CFD [29]. After obtaining the nondimensional values for different rudder angles and speeds, the analytical curves are displayed in Figure 4.

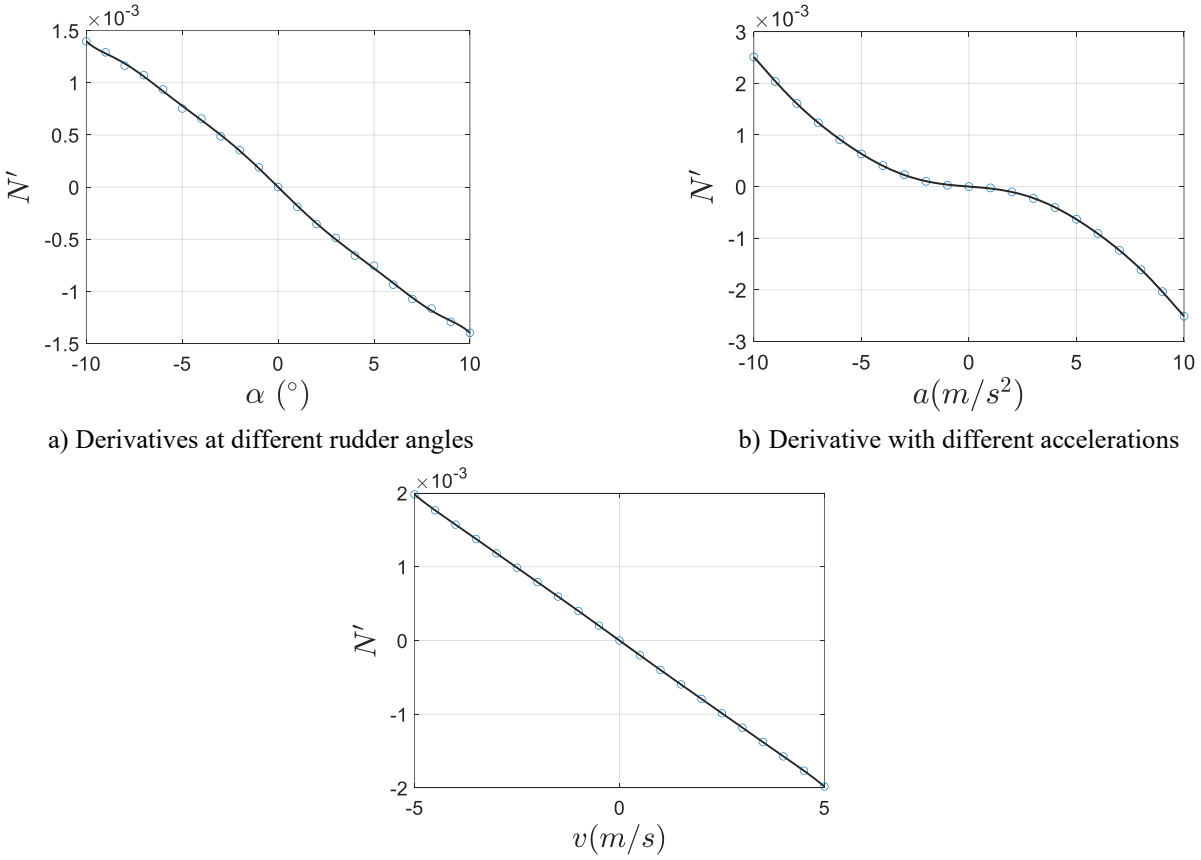

a) Derivatives at different rudder angles

b) Derivative with different accelerations

c) Derivatives at different velocities

Fig. 4 Analytical curve of derivative of velocity, rudder angle, and acceleration

Figures 5 and 6 illustrate the velocity and pressure distributions around the hull and propeller, respectively, Figure 5 depicts the vortex generated by the rotation of the tail propeller. The velocity around SUBOFF's wall surface is zero, and it's low behind the tail fin, and Figure 6 highlights high-pressure from SUBOFF's tail propeller and behind the tail fin.

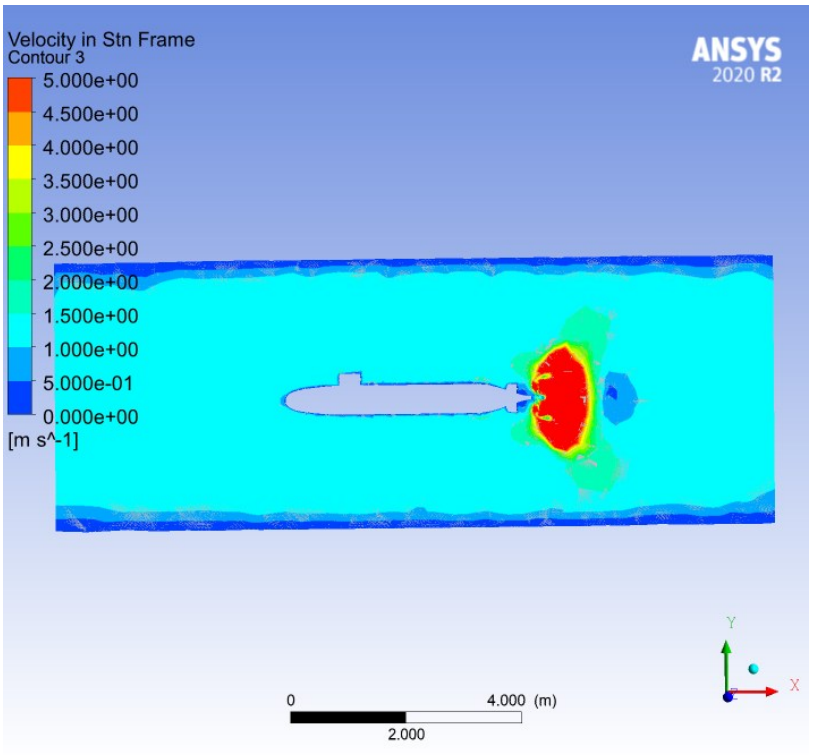

Fig. 5 Velocity distributions around the hull and propeller

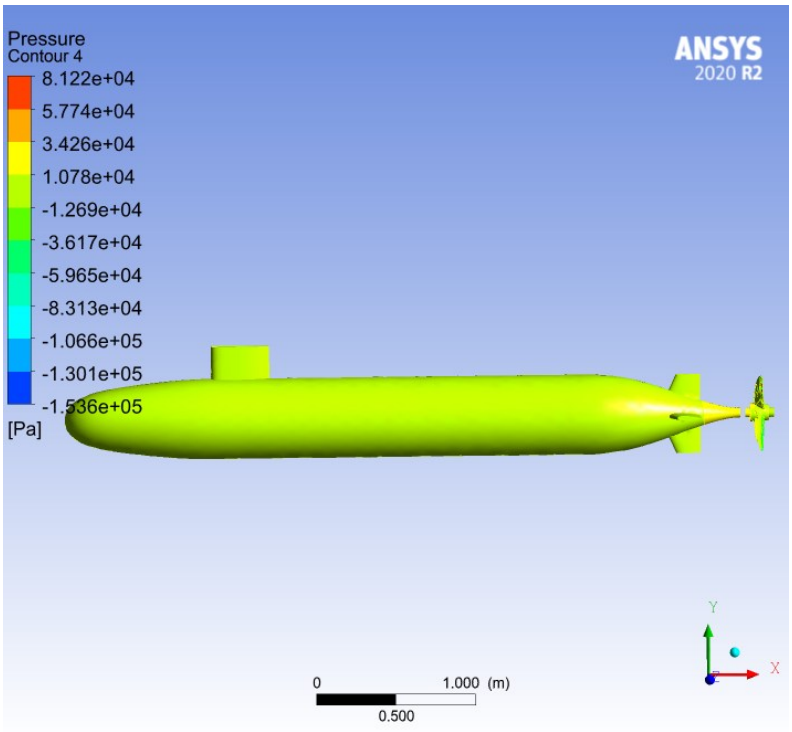

Fig. 6 Pressure distribution of SUBOFF

3.3 Structural strength

Deep-sea underwater vehicles require reliable power sources and strong pressure-resistant shells. Designing these shells to be both lightweight and durable is a challenging task. This article uses the finite element method and numerical simulation to test shell pressure resistance. The goal is to ensure strength while maintaining a lightweight design. The vehicles are assumed to operate at 1000 meters depth, with a working load 1.5 times the pressure at that depth. Specifications are detailed in Table 2.

Table 2 Pressure resistant shell parameters

Parameters	Value
Materials	7050 aluminum alloy
Load	150 Mpa
Yield limit strength	435 Mpa
Young's modulus	71 Gpa
Poisson's ratio	0.3
Material density	2860 kg/m^3
Inner radius	0.182 m
Pressure vessel thickness	0.015
Pressure vessel length	2.229 m
Rib height	0.015 m
Rib width	0.02 m
Number of ribs	10

To ensure that the pressure-resistant shell of an underwater vehicle remains intact while reducing weight, the equivalent stress and strain must stay within certain limits. The following equation must be satisfied [30]:

$$\sigma_1 \le 0.85\sigma_s \tag{12}$$

$$\sigma_2 \le 1.15\sigma_s \tag{13}$$

$$\sigma_3 \le 0.6\sigma_s \tag{14}$$

$$P_{rt} \le 1.2P_r \tag{15}$$

where σ_1 represents the circumferential stress at the midpoint of adjacent ribs, σ_2 represents the axial stress of the rib plate shell, σ_3 represents the rib stress, P_{rt} represents the critical stress of the pressure-resistant shell, P_r represents the calculated pressure. Figure 7 shows the initial state calculated stresses of the pressure-resistant shell.

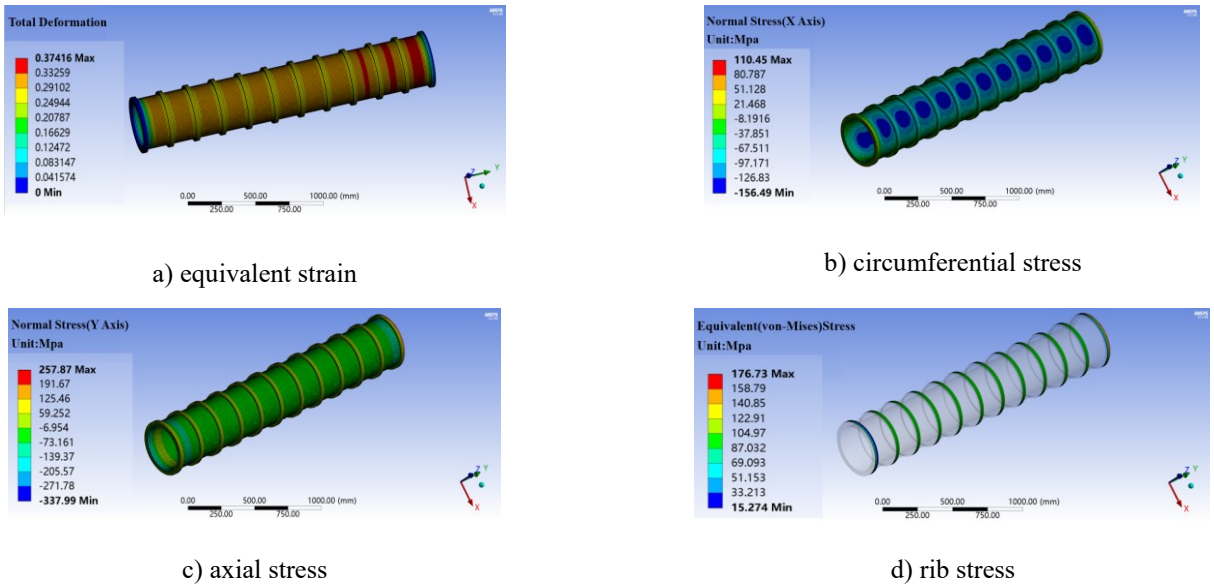

a) equivalent strain

b) circumferential stress

c) axial stress

d) rib stress

Fig. 7 Stress calculation for pressure vessel shells

3.4 Energy efficiency performance

Energy consumption often involves numerical simulations and theoretical calculations. The following is the computational expression:

$$N_e = \frac{\rho C_d S v^3}{2\eta_p} \tag{16}$$

where ρ represents fluid density, C_d is the drag coefficient, S is the wetted surface area, η_p is the propulsion efficiency coefficient.

Energy consumption mainly depends on the propulsion efficiency of the propeller. The formula for calculating propulsion efficiency is as follows:

$$\eta_p = \eta_o \eta_l \frac{1-t}{1-E_\mu} \tag{17}$$

$$\eta_l = 1.113 - 0.0464.4\sqrt{W_T} \tag{18}$$

$$W_T = \frac{C_d S}{\pi R^2 Z_r (1-E_\mu)^2 (1-t)} \tag{19}$$

where η_l denotes the propeller's relative rotation efficiency, W_T is the load coefficient, R represents the propeller radius, E_μ is the wake efficiency, Z_r indicates the number of propellers, and η_o stands for the propeller's open water efficiency:

$$E_\mu = E_p + E_f \frac{2 + 0.2\sqrt{W_T}}{1 + \sqrt{1 + W_T}} \tag{20}$$

$$t = \frac{E_\mu}{(1-E_\mu) f_t} \tag{21}$$

$$f_t = -15.7 + 29.37\sqrt{W_T} - 8.248W_T + 23.2\lambda - 39.07\sqrt{W_T}\lambda \tag{22}$$

where t is the thrust reduction coefficient, f_t is the propeller load influence coefficient, and λ is the pitch ratio at $r/R = 0.7$.

4. Optimization of dynamic proxy model.

Optimization based on proxy models has been widely applied to improve the efficiency of underwater vehicle optimization. The dynamic proxy model uses the minimum Lower Confidence Bound (LCB) for optimization and automatically generates new sampling points based on the sample space after each sample. By integrating the SMOTE with adaptive sampling, it further enhances sampling efficiency, reduces the number of samples, and improves the optimization of underwater vehicle. The initial sample points in this study were generated using a combination of optimal Latin hypercube design and orthogonal experiments. In the subsequent sampling process, oversampling techniques (SMOTE algorithm) were applied to interpolate the key sample points from the initial dataset, producing the second round of sample points. Each subsequent sampling iteration was based on the total sample set from the previous round, where key sample points were selected and interpolated to generate a new round of sample points. The collected sample points were derived through a combination of finite element methods, CFD numerical simulation, Function calculations based on the MATLAB commercial software, and theoretical analysis.

4.1. Orthogonal experimental design

Orthogonal experimental design is a parameter experiment that independently examines the sensitivity of each design factor to the response, aiming to collect a representative sample distribution. Constructing dynamic proxy models requires an adequate and efficient number of sample points. Design of Experiments (DOE) provides an effective approach for this. To improve sampling efficiency, this article employs the optimal Latin method for sample collection. The sample points were collected using CFD numerical simulation, finite element methods, and MATLAB numerical computation.

4.2. Smote algorithm

During the optimization of proxy models, samples are typically collected globally. However, a lack of sampled points near the optimal point often reduces optimization efficiency. To address this issue, this paper incorporates the SMOTE algorithm and introduces an adaptive constant to reduce the number of sample points and prevent model overfitting.

The SMOTE algorithm strategy involves selecting a concentrated sample point X_i within an interval, assuming it has N neighbors. From these N neighbors, a sample point X_j is randomly selected with K=1. By performing random interpolation between the concentrated sample point and the selected sample point, a new sample point is generated. The calculation formula is as follows:

$$X_k = X_i + rand(0,1)*(X_j - X_i) \tag{23}$$

When too many samples are collected, the sample set becomes excessively large. Randomly selecting sample points from this set may not yield optimal results. To address this, an adaptive method for collecting sample points is used. Assume the increment of the objective function at the *k*-th optimization iteration is L_p, and the actual descent value of the *i*-th model is:

$$Trued_k = g(X_i + L_p) - g(X_i) \tag{24}$$

The decrease in predicted value of the *i*-th iteration of the model is as follows:

$$Pred_k = h(X_i + L_p) - h(X_i) \tag{25}$$

The degree of approximation between the proxy model and the proxy model is:

$$r_k = \frac{Trued_k}{Pred_k} = \frac{g(X_i + L_p) - g(X_i)}{h(X_i + L_p) - h(X_i)} \tag{26}$$

If r_k is close to 1, the proxy model has high fitting accuracy. Therefore, reduce the number of neighboring samples N and add more newly generated samples to enhance local search capabilities. Conversely, if r_k is not close to 1, increase the number of neighboring samples and reduce the number of newly generated samples.

4.3. Minimum confidence lower bound criterion.

In dynamic proxy models, the method of updating pre-screening sample points significantly affects the approximation accuracy. Common methods include Expected Improvement (EI), Improvement Probability (PI), Most Likely Improvement (MI), and LCB. Among these, EI and LCB yield the best results. However, the EI criterion requires extensive local development, increasing the computational burden, whereas the LCB criterion remains effective. The objective function of LCB is defined as follows:

$$f_{rb}(x) = Pref(x) - b * \sigma(x) \tag{27}$$

where $Pref(x)$ is the predicted result of the proxy model, b is the adaptive balance constant, and $\sigma(x)$ is the standard deviation.

4.4. Optimization process of the dynamic proxy model

The optimization primarily focuses on constructing a high-accuracy dynamic proxy model and achieving efficient optimization with this model. The standard form of a nonlinear constrained optimization problem is as follows:

$$\min \ f(x)$$
$$\text{s.t.} \quad h_j(x) = 0 \quad j = 1, 2, ..., J$$
$$g_l(x) \le 0 \quad l = 1, 2, ..., L$$
$$x_{L,i} \le x_i \le x_{U,i}$$

where $x_{L,i}$ and $x_{U,i}$ are the lower and upper bounds of the design variable. The mathematical model for nonlinear problems is expressed as follows:

$$min \ f_{rb}(x) = Pref(x) - b * \sigma(x)$$
$$\text{s.t.} \ preh_j(x) = 0 \quad j = 1, 2, ..., J$$
$$preg_l(x) \le 0 \quad l = 1, 2, ..., L$$

Among them, pre denotes the proxy model for the high-accuracy objective function model.

The optimization steps of the dynamic proxy model are as follows:

(1) Establish a realistic analysis model, determine experimental variables, and set the iteration count parameter to (k=1).

(2) To ensure the spatial uniformity of the samples, the optimal Latin experimental design method is used for sampling when k=1. The response values of the real analysis model for these sample points are calculated. These sample points and their actual response values are stored in the database. The initial number of sample points N_s is selected as follows:

$$N_s = min\left\{\frac{(n_v+1)(n_v+2)}{2}, 5n_v\right\} \tag{28}$$

(3) When (k>1), use the SMOTE algorithm to perform random sampling around the optimal point. Calculate the actual response values of the sampled points and store them in the database.

(4) Construct an RBF proxy model using the sample points in the database. Establish a balancing constant based on the prediction error.

(5) Use a combined optimization algorithm based on a genetic algorithm and NLPQLP algorithm to perform global and local optimization using the proxy model starting from step (4). Obtain the optimal parameters X and the optimal value $Y(X)$ for the k-th iteration.

(6) Substitute the optimal parameters X from the k-th iteration into the actual model. Solve for the actual response value. Store the response value in the database.

(7) Calculate the relative error between the actual response value of the k-th potential optimal solution and the actual response value of the (k-1)st potential optimal solution during the optimization process. Check if it converges. If it does not converge, return to step (8). If it converges, the iteration ends, and the optimal value is output. The convergence relative error is set at 3% due to the integration of four disciplines.

(8) Calculate the balance constant of the SMOTE algorithm. As the balance constant r_k approaches 1, reduce the number of neighboring samples (N) and increase the number of newly generated samples to enhance global search ability. Conversely, increase the number of neighboring samples and reduce the number of newly generated samples. Increment the iteration parameter ($k = k + 1$) and return to step (3).

The flow chart is shown in Figure 8.

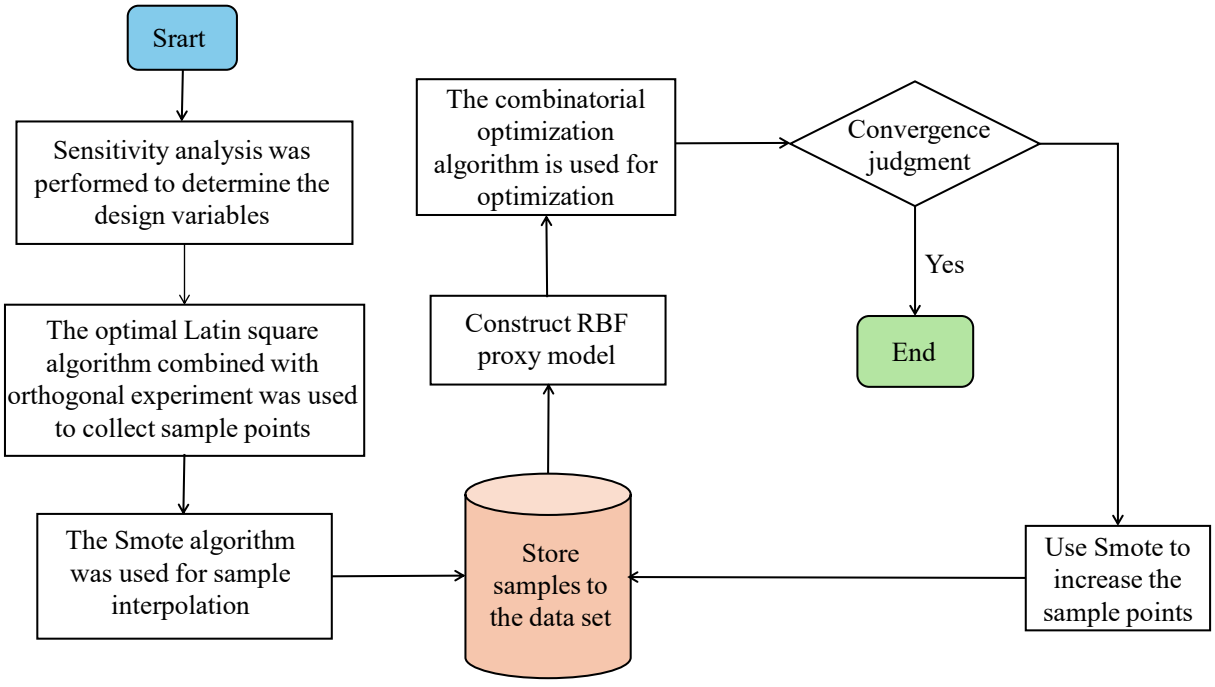

Fig. 8 Dynamic proxy model optimization flow chart

5. Multidisciplinary integrated optimization

5.1 Collaborative optimization method

The most classic optimization methods include the Multidisciplinary Feasible Direction method (MDF) [31], the Collaborative Optimization method (CO) [32], the Two-Level System Synthesis method (BLISS) [33], and the Multidisciplinary MDF. The optimization process requires extensive system

and disciplinary analysis. However, the robustness of the BLISS is inadequate for highly nonlinear multidisciplinary optimization problems. Therefore, the CO has proven feasible for the multidisciplinary optimization design of underwater vehicles with multiple parameters and dimensions [15].

A correlation table was used to analyze the sensitivity of parameters, helping to identify key parameters and reduce the number of target parameters.

Sensitivity analysis uses statistical methods, such as analysis of variance and regression analysis, to determine how design parameters impact system output. The principle of sensitivity analysis is as follows:

Assuming the model is composed of multivariable functions, the model is as follows:

$$Y = g(x_1, x_2, ..., x_n) = g_0 + \sum_{i=1}^{n} g_i(x_i) + \sum_{i<j} g_{ij}(x_i, x_j) + g_{1,2,...,n}(x_1, x_2, ..., x_n) \tag{29}$$

where $g(x_1, x_2, ..., x_n)$ is a function of the multidimensional variable $(x_1, x_2, ..., x_n)$.

The total function considers the interaction of single parameter variables, and the total variance can be decomposed into the variance of individual parameters, as shown below:

$$V(Y) = \sum_{i=1}^{n} v_i + \sum_{i=1}^{n} \sum_{j=i+1}^{n} (v_{ij} + \cdots + v_{i,j,...,n}) \tag{30}$$

where $V(Y)$ represents the total variance, v_i denotes the first-order variance of x_i with respect to Y, v_{ij} is the variance resulting from the interaction between x_i and x_j, and $v_{i,j,...,n}$ represents the variance caused by the interaction of all parameters.

The dimensionless variance $\overline{V}$ is expressed by the following formula:

$$\overline{V_i} = \frac{v_i}{V(Y)} \tag{31}$$

$$\overline{V_{ij}} = \frac{v_{ij}}{V(Y)} \tag{32}$$

$$\overline{V}_{i,j,...,n} = \frac{v_{i,j,...,n}}{V(Y)} \tag{33}$$

The sensitivity coefficients for the linear terms, interaction terms, and quadratic terms are determined by the following formulas:

$$S_\alpha = \frac{\partial Y}{\partial x_i^2}, i = 1, ..., n \tag{34}$$

$$S_\beta = \frac{\partial Y}{\partial x_i}, i = 1, ..., n \tag{35}$$

$$S_\gamma = \frac{\partial Y}{\partial (x_k ... x_l)}, k \in (1, n-1), l \in (2, n), k < l \tag{36}$$

where S_α represents the sensitivity coefficient for the quadratic term, S_β for the linear term, and S_γ for the interaction term.

The parameters used were the minimum rear body radius (rh), tail smoothness index (Kl), maximum radius (R_{max}), parallel midship body length (L), pressure-resistant shell thickness (h_1), shell rib height (h_2), and shell rib width (Wd). Sensitivity analysis was conducted on resistance, mass, yaw moment, and energy consumption, as shown in Figure 9.

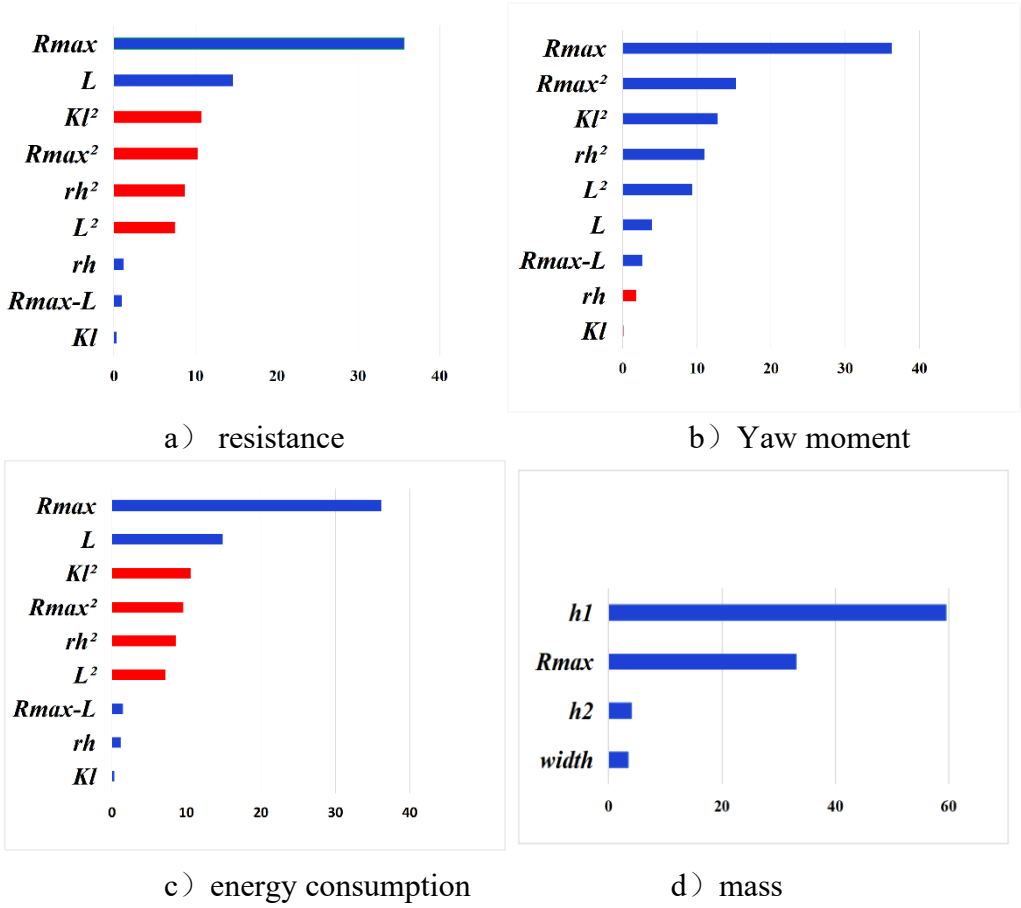

Fig. 9 Parameter sensitivity analysis

The collaborative optimization framework includes a system set and multiple discipline sets, as shown in Figure 6. Sensitivity analysis can be used to design the objective function of each discipline set. the main goal for the discipline of rapidity is to minimize resistance. The design parameters include the linear terms Rmax and L, and the objective function can be formulated as follows:

$$f_1 = (R_{\max 1} - R_{\max})^2 + (L_1 - L)^2 \tag{37}$$

In the field of maneuverability, the K and T indices are calculated to enhance underwater vehicle performance by reducing yaw moment. Considering the correlation with other disciplines, both cross terms and linear terms of R_{max} and L are selected. The objective function can be designed as follows:

$$f_2 = (R_{\max 2} - R_{\max})^2 + (L_2 - L)^2 + (R_{\max 2} - L_2 - R_{\max} + L)^2 \tag{38}$$

In structural strength discipline, the parameters are the maximum radius R_{max}, shell thickness h_1, rib width $h2$, and rib spacing Wd. The objective function is as follows:

$$f_3 = (R_{\max 3} - R_{\max})^2 + (h_{13} - h_1)^2 + (h_{23} - h_2)^2 + (W_{d3} - W_d)^2 \tag{39}$$

In energy consumption, resistance shows a strong correlation. Therefore, the linear terms R_{max}, rh, and L, along with the cross term R_{max} - L, are chosen for the objective function, which can be formulated as follows:

$$f_4 = (R_{\max 4} - R_{\max})^2 + (L_4 - L)^2 + (R_{\max 4} - L_4 - R_{\max} + L)^2 \tag{40}$$

Using AHP and expert ratings, the main subject set function is derived from the weight formula (Pan and Luo,2024). The objective function for the system set can be designed as follows:

$$f = 0.1175F_d + 0.27787Y + 0.06947M + 0.05496N_e + 0.48006m \tag{41}$$

Here, F_d is resistance, Y is the transverse force, M is the yaw moment, N_e is the energy consumption, and m is the mass.

5.2 Optimization results

The optimization stops when the difference between the current optimal value and the previous value falls below 0.001. This study used a combined optimization method, with a genetic algorithm for global optimization and the NLPQLP algorithm for local optimization. The SUBOFF speed for the underwater vehicle was set to 10.58 knots, and the drift angle was set at 7 degrees. Figure 10 shows the optimization results: black dots for feasible points, blue dots indicate suboptimal points, red dots for infeasible points, and green dots for optimal points, The iteration consists of 720 steps, and the optimal solution appears at step 711. To verify the advantages of the proposed dynamic proxy model over other proxy models, one static proxy model (L-SRBF) and two dynamic proxy models (L-LCB-DRBF and L-TR-DRBF) were compared. The L-LCB-DRBF model is a dynamic proxy model that uses an adaptive balancing constant and the LCB criterion. The L-TR-DRBF model is a dynamic proxy model that uses the trust region method. At the optimal point, the errors between predicted results and the actual responses are calculated and listed in Table 3. The predicted results are obtained from proxy models. The actual responses are obtained thought CFD calculation. As shown, the proposed L-DRBF dynamic surrogate model exhibits the highest optimization efficiency and minimal errors under 1 %. Although the L-TR-DRBF model achieves the comparable fitting accuracy, the optimization efficiency is worse than the proposed model. The NLPQLP algorithm, a gradient-based search method, demonstrates its advantage in rapidly finding the optimal solution within a local range after achieving global optimization. Compared to the Multi-Island Genetic Algorithm (MIGA), which requires 1000 iterations to converge, the NLPQLP algorithm achieves convergence in just 46 iterations. This highlights its remarkable optimization efficiency.

Table 3 Comparison between different proxy models

Proxy model	Model calls	Yaw moment	Mass	Resistance	Energy consumption	Transverse force
L-DRBF	84	0.0232%	0.065%	0.0081%	0.1%	0.385%
L-SRBF	134	0.876%	2.439%	4.645%	2.203%	1.171%
L-LCB-DRBF	91	2.23%	0.848%	0.703%	0.83%	0.673%
L-TR-DRBF	93	0.0283%	0.0625%	0.00548%	0.0486%	0.0124%

Table 4 shows the ranges of various parameters for the underwater vehicles, along with the optimized values. The yawing moment, resistance, and mass have significantly decreased after weight reduction in the SUBOFF, resulting in improved maneuverability. However, the reduced yawing moment alone does not fully represent the maneuvering performance of the SUBOFF vehicle. Therefore, the K and T indices need to be calculated using the optimized parameters and compared with those obtained under the initial conditions.

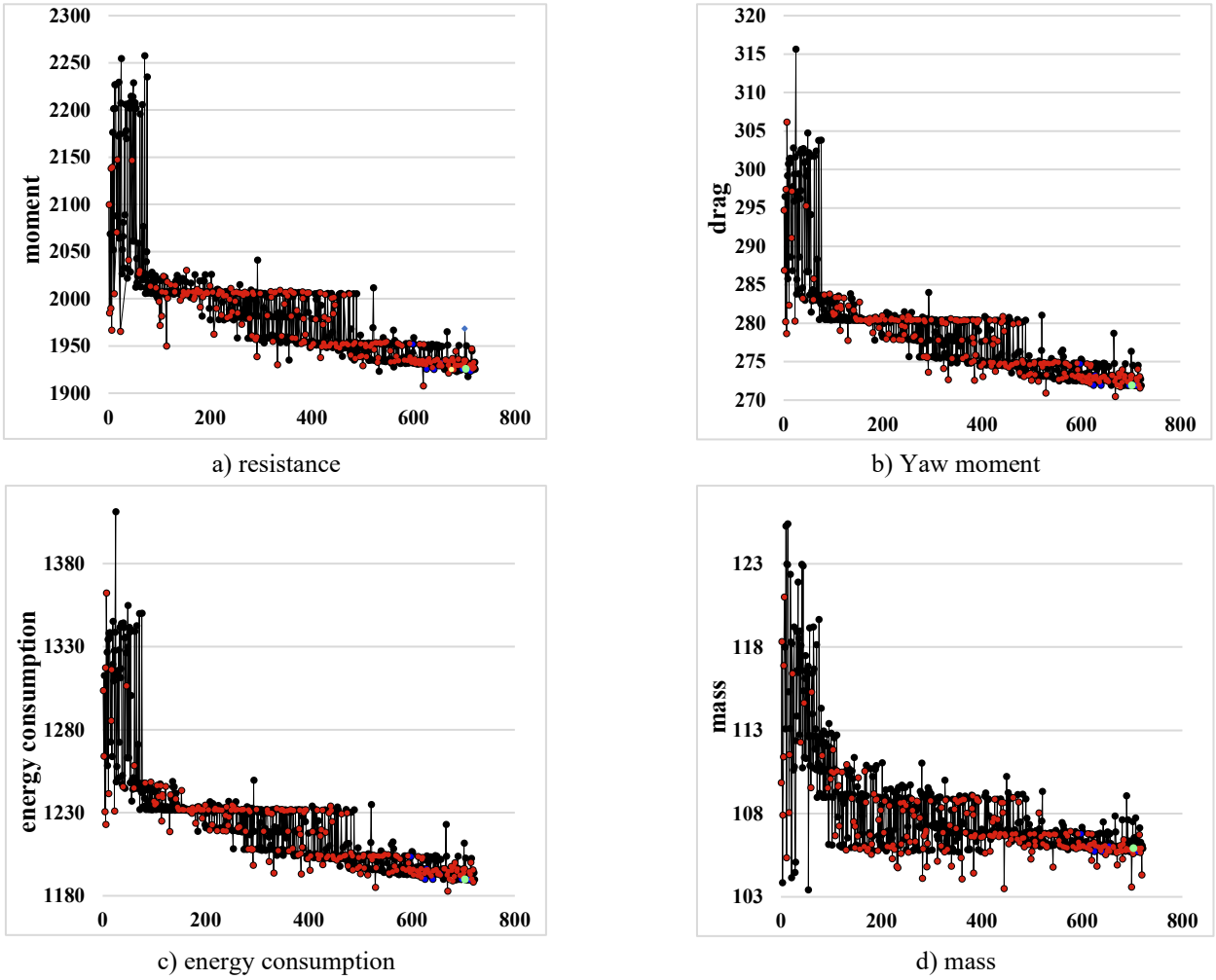

a) resistance b) Yaw moment

c) energy consumption d) mass

Fig. 10 Optimization process of system set and subject set

Table 4 Comparison of optimization results

	Initial value	Range	Optimized value
L (Ft)	7.3125	[6.9479,7.6781]	6.9805
R_{max} (Ft)	0.833333	[0.7917,0.875]	0.792
rh (Ft)	0.1175	[0.1,0.2]	0.13914
Kl (Ft)	44.6244	[42.3932,46.8556]	44.6735
h_1 (m)	0.015	[0.012,0.015]	0.01292
h_2 (m)	0.015	[0.01425,0.01575]	0.01574
W_d (m)	0.02	[0.019,0.021]	0.01931
N_e (N·m/s)	1291.2075		1190 (-7.84%)
F_d (N)	292.269		271.9 (-6.97%)
Mass (kg)	126.6257		105.93 (-16.34%)
T	11.339		10.892
K	0.4281		0.4309

Figure 11 shows the line shape and planing surface of the SUBOFF underwater vehicle before and after optimization. Changes in the maximum radius, length, and tail profile thickness have been observed. These results demonstrate the feasibility of the optimization. The red line represents the optimized version, while the black line represents the original version.

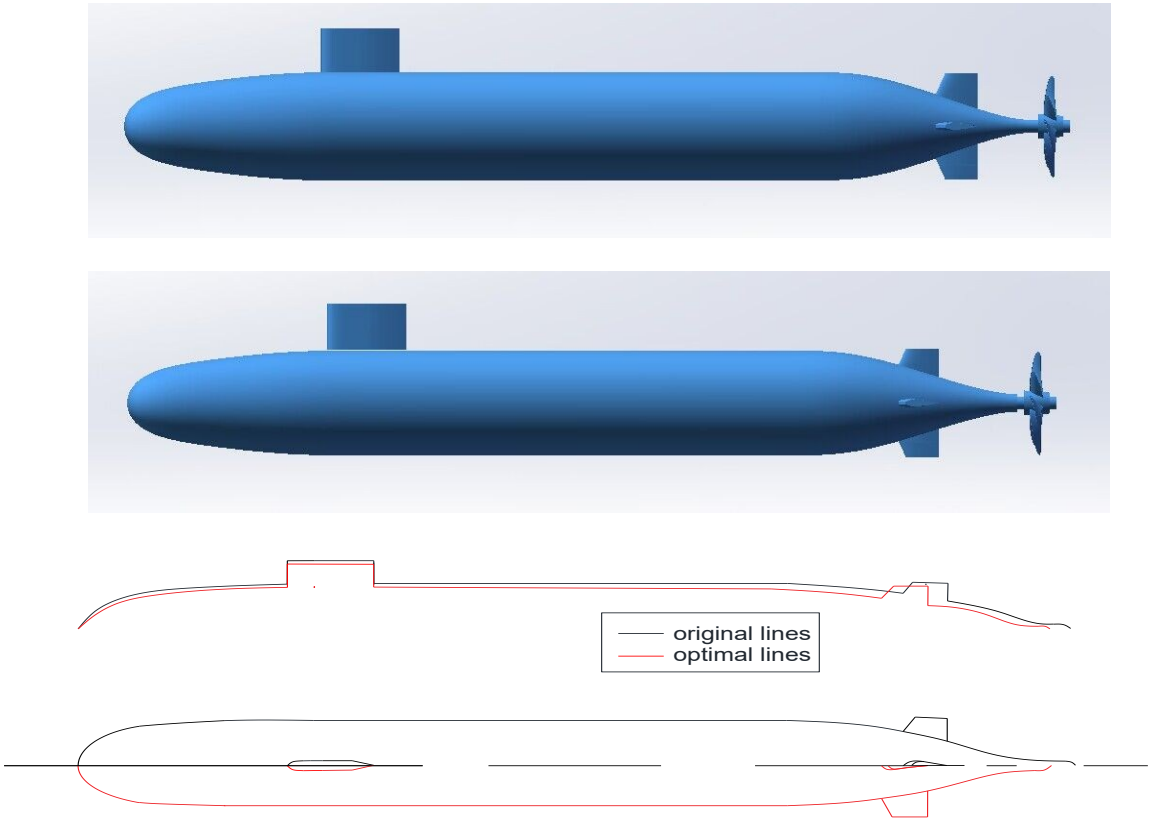

Fig. 11 Comparison of the geometric model of SUBOFF before and after optimization

6. Conclusion

In the study of the application of MDO to an underwater vehicle. The focus is primarily on using proxy models within a collaborative optimization framework to build a hybrid optimization strategy. The results of the optimization indicate that:

(1) A multidisciplinary optimization platform combining the NSGA-II genetic algorithm and the NLPQLP algorithm within a collaborative optimization framework has demonstrated feasibility when applied to underwater vehicles.

(2) Using CFD numerical simulation, data can be efficiently obtained. These data can then be used to derive the K and T indices, which can effectively evaluate the maneuvering performance of underwater vehicles.

(3) The sampling strategy of the proposed dynamic proxy model establishes confidence intervals at optimal points, interpolates near key points, and timely adjusts these confidence intervals in a timely manner. Compared to other dynamic proxy models, this approach enhances optimization efficiency.

In this study, the propeller angle was adjusted to determine the K and T indices. Future research will focus on adjusting the tail fin angle to calculate the maneuverability of the underwater vehicle. The K and T indices are merely one measure of maneuverability and cannot fully capture the overall maneuvering performance of an underwater vehicle under complex sea conditions. Moreover, the dynamic proxy model proposed in this paper incorporates multiple sophisticated methods, making it challenging to generalize to the design of ships, airfoils, and similar applications. Currently, this optimization framework is specifically tailored for underwater vehicles. Future research will focus on employing more advanced techniques to better capture the maneuvering performance of underwater vehicles and explore the use of ensemble surrogate models to enhance the generalization capability of the proxy model.

ACKNOWLEDGEMENTS

This work was supported by the Natural Science Foundation of Fujian Province of China [No. 2023J011572], and the Fujian Science and Technology Major Special Project [2022NZ033023].

REFERENCES

[1] Zhou, Q., Jiang, P., Xu, H., Chen, L., Huang, W., 2016. Application of improved multi-discipline collaborative optimization in ship conceptual design based on dynamic penalty factors. *Journal of ship mechanics*, 20(10), 1269-1280.

[2] Hart, C. G., Vlahopoulos, N., 2010. An integrated multidisciplinary particle swarm optimization approach to conceptual ship design. *Structural and Multidisciplinary Optimization*, 41, 481-494. https://doi.org/10.1007/s00158-009-0414-0

[3] Zhang, H., 2015. Application of multidisciplinary design optimization to ship design. *Ship Science and Technology*, 37(6), 87-91.

[4] Gholinezhad, H., Torabi, S. H., 2022. Reliability-based multidisciplinary design optimization of an underwater vehicle including cost analysis. *Journal of Marine Science & Technology*, 27(1), 11-26. https://doi.org/10.1007/s00773-021-00804-2

[5] Mikulec, M., Piehl, H., 2023. Verification and validation of CFD simulations with full-scale ship speed/power trial data. *Brodogradnja*, 74(1), 41-62. https://doi.org/10.21278/brod74103

[6] Liu, J., Feng, G., Wang, J., Wu, T., Xu, C., Yang, K., 2024. Research on temperature distribution in container ship with Type-B LNG fuel tank based on CFD and analytical method. *Brodogradnja*, 75(3), 75302. https://doi.org/10.21278/brod75302

[7] Bal, K., Bural, D. B., 2024. Investigation into forces on offshore piles with constant and linearly varying diameters using CFD and extended Morison equation under separate wave and current loadings. *Brodogradnja*, 75(4), 75406. https://doi.org/10.21278/brod75406

[8] Alvarez, A., Bertram, V., Gualdesi, L., 2009. Hull hydrodynamic optimization of autonomous underwater vehicles operating at snorkeling depth. *Ocean Engineering*, 36(1), 105-112. https://doi.org/10.1016/j.oceaneng.2008.08.006

[9] Gao, T., Wang, Y., Pang, Y., Cao, J., 2016. Hull shape optimization for autonomous underwater vehicles using CFD. *Engineering Applications of Computational Fluid Mechanics*, 10(1), 599-607. https://doi.org/10.1080/19942060.2016.1224735

[10] Ignacio, L., Victor, R., Del Rio, R., Pascoal, A., 2019. Optimized design of an autonomous underwater vehicle, for exploration in the Caribbean Sea. *Ocean Engineering*, 187, 106184. https://doi.org/10.1016/j.oceaneng.2019.106184

[11] Alam, K., Ray, T., Anavatti, S., 2014. Design and construction of an autonomous underwater vehicle. *Neurocomputing*, 142, 16-29. https://doi.org/10.1016/j.neucom.2013.12.055

[12] Alam, K., Ray, T., Anavatti, S., 2015. Design optimization of an unmanned underwater vehicle using low-and high-fidelity models. *IEEE Transactions on Systems, Man, and Cybernetics: Systems*, 47(11), 2794-2808. https://doi.org/10.1109/TSMC.2015.2390592

[13] Tian, W., Mao, Z., Zhao, F., Zhao, Z., 2017. Layout optimization of two autonomous underwater vehicles for drag reduction with a combined CFD and neural network method. *Complexity*, 2017(1), 5769794. https://doi.org/10.1155/2017/5769794

[14] Li, B., Pang, Y., Cheng, Y., Zhu, X., 2017. Collaborative optimization for ring-stiffened composite pressure hull of underwater vehicle based on lamination parameters. *International Journal of Naval Architecture and Ocean Engineering*, 9(4), 373-381. https://doi.org/10.1016/j.ijnaoe.2016.09.009

[15] Lyu, W., Luo, W., 2014. Design of underwater robot lines based on a hybrid automatic optimization strategy. *Journal of Marine Science and Application*, 13, 274-280. https://doi.org/10.1007/s11804-014-1257-7

[16] Yang, M., Zhang, D., Wang, F., Han, X., 2022. Efficient local adaptive Kriging approximation method with single-loop strategy for reliability-based design optimization. *Computer Methods in Applied Mechanics and Engineering*, 390, 114462. https://doi.org/10.1016/j.cma.2021.114462

[17] Wang, P., Feng, Y., Chen, Z., Dai, Y., 2023. Study of a hull form optimization system based on a Gaussian process regression algorithm and an adaptive sampling strategy, Part II: Multi-objective optimization. *Ocean Engineering*, 286, 115501. https://doi.org/10.1016/j.oceaneng.2023.115501

[18] Chen, H., Li, W., Cui, W., Liu, Q., 2022. A pointwise ensemble of surrogates with adaptive function and heuristic formulation. *Structural and Multidisciplinary Optimization*, 65(4), 113. https://doi.org/10.1007/s00158-022-03202-3

[19] Luo, W., Guo, X., Dai, J., Rao, T., 2021.Hull optimization of an underwater vehicle based on dynamic proxy model. *Ocean Engineering*, 230, 109050. https://doi.org/10.1016/j.oceaneng.2021.109050

[20] Pan, W., Luo, W., 2024. Lines optimisation of an underwater vehicle using SMOTE and adaptive minimise LCB based dynamic proxy models. Ships and Offshore Structures, 19(1), 91-108. https://doi.org/10.1080/17445302.2022.2143631

[21] Liu, J., Wu, S., Yue, X., Yue, Q., 2024. Hydrodynamic shape optimization of an autonomous and remotely-operated vehicle via a multi-surrogate model. *Brodogradnja*, 75(3), 75301. https://doi.org/10.21278/brod75301

[22] Carrica, P. M., Castro, A. M., Stern, F., 2010. Self-propulsion computations using a speed controller and a discretized propeller with dynamic overset grids. *Journal of marine science and technology*, 15, 316-330. https://doi.org/10.1007/s00773-010-0098-6

[23] Choi, J. E., Min, K. S., Kim, J. H., Lee, S. B., Seo, H. W., 2010. Resistance and propulsion characteristics of various commercial ships based on CFD results. *Ocean engineering*, 37(7), 549-566. https://doi.org/10.1016/j.oceaneng.2010.02.007

[24] Ghassemi, H., Ghadimi, P., 2008. Computational hydrodynamic analysis of the propeller–rudder and the AZIPOD systems. *Ocean Engineering*, 35(1), 117-130. https://doi.org/10.1016/j.oceaneng.2007.07.008

[25] Wu, X. C., Wang, Y. W., Huang, C. G., Hu, Z. Q., Yi, R. W., 2015. An effective CFD approach for marine-vehicle maneuvering simulation based on the hybrid reference frames method. *Ocean Engineering*, 109, 83-92. https://doi.org/10.1016/j.oceaneng.2015.08.057

[26] Wu, P. C., 2022. CFD Body Force Propeller Model with Blade Rotational Effect. *Applied Sciences*, 12(21), 11273. https://doi.org/10.3390/app122111273

[27] Ardeshiri, S., Mousavizadegan, S. H., 2022.An efficient method to calculate the maneuvering coefficient of underwater vehicles. *Ocean Engineering*, 266, 113168. https://doi.org/10.1016/j.oceaneng.2022.113168

[28] Chase, N., Carrica, P. M., 2013. Submarine propeller computations and application to self-propulsion of DARPA Suboff. *Ocean Engineering*, 60, 68-80. https://doi.org/10.1016/j.oceaneng.2012.12.029

[29] Zhang, Z., Sun, P., Pan, L., Zhao, T.,2024. On the propeller wake evolution using large eddy simulations and physics-informed space-time decomposition. *Brodogradnja*, 75(1), 1-21. https://doi.org/10.21278/brod75102

[30] Zhou, H., 2021. Research on Integrated Optimal Method of Polar AUV. China, Harbin Engineering University.

[31] Adelman, H. M., Mantay, W. R., 1991. Integrated multidisciplinary design optimization of rotorcraft. *Journal of Aircraft*, 28 (1), 22–28. https://doi.org/10.2514/3.45988

[32] Kroo, I., Altus, S., Braun, R., Gage, P, Sobieski, I., 1994. Multidisciplinary Optimization Methods for Aircraft Preliminary Design. *5th Symposium on Multidisciplinary Analysis and Optimization*, Panama City Beach, Florida, 697–707. https://doi.org/10.2514/6.1994-4325

[33] Sobieszczanski-Sobieski, J., Agte, J. S., Sandusky, R. R., 2000. Bilevel integrated system synthesis. *AIAA Journal*, 38(1), 164–172. https://doi.org/10.2514/2.937